

Supporting Information for:

Hyperspectral imaging of structure and composition in atomically thin heterostructures

Robin W. Havener¹, Cheol-Joo Kim², Lola Brown², Joshua W. Kevek³, Joel D. Sleppy¹, Paul L. McEuen^{3,4}, Jiwoong Park^{2,4}

1. School of Applied and Engineering Physics, Cornell University, Ithaca, NY 14853
2. Department of Chemistry and Chemical Biology, Cornell University, Ithaca, NY 14853
3. Laboratory for Atomic and Solid State Physics, Cornell University, Ithaca, NY 14853
4. Kavli Institute at Cornell for Nanoscale Science, Cornell University, Ithaca, NY 14853

1. DUV-Vis-NIR microscope

To maintain DUV compatibility and remove chromatic aberrations in our hyperspectral microscope, we eliminated all refractive elements and non-DUV-compatible glass (such as BK7) from the light path; additionally, all reflective elements are made from DUV-enhanced aluminum. We use a UV enhanced 1000 W Xe arc source (Optical Building Blocks Corp.) with a monochromator (2 nm spectral resolution) to select a specific wavelength. Light exiting the monochromator is focused with parabolic mirrors into a solarization-resistant multimode fiber, which delivers the light to the microscope. In reflection mode, a DUV 50/50 beamsplitter (Acton) directs the light to critically illuminate the sample with a spot size of $\sim 70 \mu\text{m}$ through a reflective (Schwarzschild) objective with an N.A. of 0.65, an effective magnification of $\sim 100\times$, and spatial resolution of $\sim \lambda$ (see below). In transmission mode, a second reflective objective acts as a condenser. All images are normalized with respect to a bare substrate to correct for variations in illumination intensity. For wavelengths below 250 nm, an additional DUV bandpass filter (Acton) is required to remove stray light at longer wavelengths, which originates from the monochromator and/or fiber. For wavelengths from 500-1000 nm, a single long pass filter may be used to remove second order diffracted light from the monochromator. Our CCD detector is UV enhanced, allowing detection from 200-1000 nm.

2. Spatial resolution

The central mirror of a Schwarzschild objective obscures the central portion of the collected light cone (see Fig 1c, main text). The result for imaging is that the performance of the objective is somewhat degraded, compared to that of a refractive objective with the same N.A., when imaging larger features ($> \lambda/\text{N.A.}$ for our objective, which has an obscuration of 16.7%). However, the performance of both reflective and refractive objectives with the same N.A. is approximately the same close to the Abbe diffraction limit (feature size of $\lambda/2\text{N.A.}$)¹. The Abbe limit for a refractive objective with N.A. = 0.65 is 0.77λ , and so we approximate the resolution of our reflective objective as λ (30% larger) in the main text.

3. Sample fabrication

Graphene/*h*-BN heterojunctions are produced using the patterned regrowth method². First, graphene is grown on copper foil, using previously reported CVD techniques³, in a hot wall tube furnace while flowing 100 sccm of H₂ and 6 sccm of CH₄ at 1000°C. Next, the graphene is patterned using standard photolithography techniques, and *h*-BN is immediately regrown on the same sample at 1000°C by sublimation of ammonia borane in a separate heating zone (at 95°C for the G/*h*-BN sample in Figs 2 & 3, 75°C in Fig 5) with 100 sccm of H₂. For tBLG, large grain graphene growths are conducted either in a copper enclosure that is inserted into the furnace⁴, annealed under 12 sccm of H₂ for 3 hours, and grown with the addition of 2 sccm of CH₄ at 980°C (Fig 4); or by using a procedure reported by Bi *et al.*⁵ (Fig 5).

To transfer these samples to other substrates, PMMA (poly(methylmethacrylate), 2% 495K in anisole) is spin-coated on the copper/sample; then, either the uncoated side is floated on a dilute aqueous iron(III) chloride solution, etching the copper from the back (tBLG and G/*h*-BN sample in Fig 5), or the PMMA/sample membrane is electrochemically delaminated from the copper (G/*h*-BN sample in Figs 2 & 3)⁶. The remaining PMMA/sample membrane is washed with copious amounts of water and transferred to the target substrate. Samples on TEM grids (TEM Windows, #SN100-A10Q33) are annealed in air

(325°C, 3 hours) to remove PMMA. Samples on silicon are dried to remove remaining water, and the PMMA is removed with acetone.

4. Calculation of σ

To calculate the complex σ of our atomically thin samples, we model our substrate + sample as a series of thin films using the transfer matrix formalism⁷, and solve simultaneously for the values of $\text{Re}[\sigma]$ and $\text{Im}[\sigma]$ which best fit our transmission and reflection data. We set the incident angle of the unpolarized light in our model to 30° from the normal (which is the average incident angle produced by our reflective objective), and we assume that a single layer of graphene or *h*-BN has a thickness of 0.34 nm, close to the interplanar spacing of both materials^{8,9}.

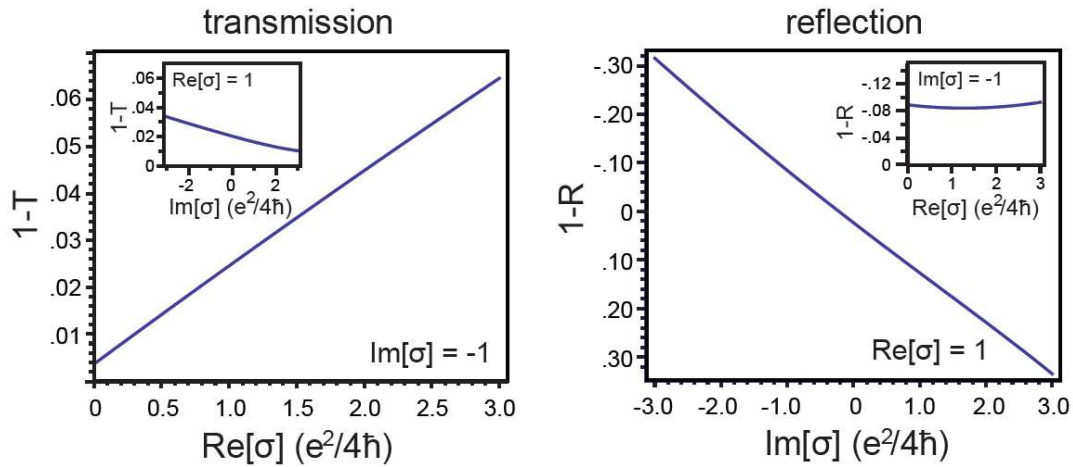


Figure S1: Calculated contrast for an atomically thin film in (left) transmission and (right) reflection mode on a 10 nm thick silicon nitride membrane. For transmission (reflection) mode, the contrast is plotted as a function of $\text{Re}[\sigma]$ ($\text{Im}[\sigma]$) while $\text{Im}[\sigma]$ ($\text{Re}[\sigma]$) is held constant. In the insets, $\text{Im}[\sigma]$ ($\text{Re}[\sigma]$) varies while $\text{Re}[\sigma]$ ($\text{Im}[\sigma]$) is constant.

In the main text, we assert that the contrast of an atomically thin film on a SiN membrane in transmission mode is approximately proportional to $\text{Re}[\sigma]$ of the film, while in reflection mode it is approximately proportional to $\text{Im}[\sigma]$. Figure S1 shows the calculated contrast of an atomically thin (0.34 nm) film in transmission and reflection modes on a 10 nm thick SiN membrane at 2.5 eV as a function of

$\text{Re}[\sigma]$ and $\text{Im}[\sigma]$ of the atomically thin film. This calculation demonstrates that there is an approximately linear relationship between contrast and $\text{Re}[\sigma]$ in transmission mode, and between contrast and $\text{Im}[\sigma]$ in reflection mode. Additionally, there is much less variation in contrast when the opposite parameter ($\text{Im}[\sigma]$ in transmission mode or $\text{Re}[\sigma]$ in reflection mode) is varied.

We also find it necessary to add an additional layer to our thin film model to account for material trapped under the 2D film and/or adsorbates¹⁰, with a thickness of 1-2 nm, to obtain consistent and reasonable results (examples of which are discussed below) when calculating σ of the atomically thin film. Adding this extra layer effectively increases our calculated value of $\text{Im}[\sigma]$ by a constant, with little effect on $\text{Re}[\sigma]$.

For simplicity, we assume that the debris is only trapped under the film, not adsorbed on top of it, and that $\sigma(\lambda)$ of the debris is that of PMMA¹¹. We choose the thickness of the debris layer such that our calculated $\text{Im}[\sigma]$ of the atomically thin film meets several criteria: 1. $\text{Im}[\sigma]$ of Bernal-stacked bilayer graphene is approximately twice that of single-layer graphene, when applicable; 2. The real part of the permittivity ($\epsilon = i\sigma/\omega$) is roughly constant as a function of energy away from a resonance; 3. The real part of the refractive index $n = \text{Re}[\epsilon^{1/2}]$ at low energies is consistent with literature values for single-layer graphene⁸ and bulk *h*-BN¹². Without the extra layer in our model, these criteria are not met.

The debris thicknesses that best meet these criteria are 1 nm for the tBLG sample, as well as the *h*-BN within the graphene/*h*-BN lateral heterojunction, and 2 nm for the graphene within the same lateral heterojunction. While it may seem unusual that different amounts of debris are associated with graphene and *h*-BN in the same sample, this assertion is corroborated by a bright-field TEM image of the junction, which shows more debris associated with the graphene (Figure S2).

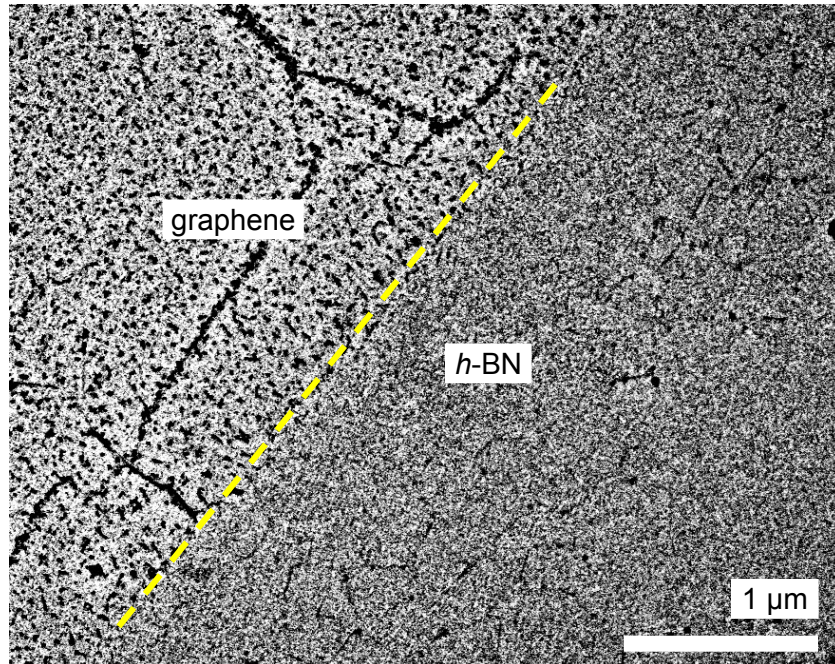


Figure S2: Bright-field TEM image of the graphene/*h*-BN junction. Dark particles (opaque to the electron beam) are trapped on or under the graphene which are not present on the *h*-BN side of the junction.

This debris layer introduces uncertainty into our calculation of $\text{Im}[\sigma]$ for our atomically thin film. Particularly, the dispersion of the debris is unknown, and this will likely introduce the greatest uncertainty in $\text{Im}[\sigma]$ at high energies where the dispersion of different insulating materials can vary greatly. Full Kramers-Kronig analysis¹³ may be useful in the future to find a consistent $\sigma(\lambda)$ for all materials present.

References

- 1 Nadorff, G. & DeWitt, F. Reflexicon objectives for imaging, <https://cvimellesgriot.com/products/Documents/TechnicalGuide/CVIMGReflexicon_Whitepaper.pdf> **2012**.
- 2 Levendorf, M. *et al.* Graphene and boron nitride lateral heterostructures for atomically thin circuitry. *Nature* **2012**, *488*, 627-632.
- 3 Li, X. *et al.* Large-Area Synthesis of High-Quality and Uniform Graphene Films on Copper Foils. *Science* **2009**, *324*, 1312-1314.
- 4 Li, X. *et al.* Large-Area Graphene Single Crystals Grown by Low-Pressure Chemical Vapor Deposition of Methane on Copper. *J. Am. Chem. Soc.* **2011**, *133*, 2816-2819.
- 5 Bi, H. *et al.* The production of large bilayer hexagonal graphene domains by a two-step growth process of segregation and surface-catalytic chemical vapor deposition. *Carbon* **2012**, *50*, 2703-2709.

- 6 Wang, Y. *et al.* Electrochemical Delamination of CVD-Grown Graphene Film: Toward the
Recyclable Use of Copper Catalyst. *ACS Nano* **2011**, *5*, 9927-9933.
- 7 Roddaro, S., Pingue, P., Piazza, V., Pellegrini, V. & Beltram, F. The optical visibility of
graphene: Interference colors of ultrathin graphite on SiO₂. *Nano Lett.* **2007**, *7*, 2707-2710.
- 8 Blake, P. *et al.* Making graphene visible. *Appl. Phys. Lett.* **2007**, *91*, 063124.
- 9 Shi, Y. *et al.* Synthesis of Few-Layer Hexagonal Boron Nitride Thin Film by Chemical Vapor
Deposition. *Nano Lett.* **2010**, *10*, 4134-4139.
- 10 Bruna, M. & Borini, S. Assessment of graphene quality by quantitative optical contrast analysis.
J. Phys. D: Appl. Phys. **2009**, *42*, 175307.
- 11 Ispirian, M., Karabekyan, S. & Eckmann, R. Cyro Industries Inc. data tabulated by luxpop.com,
<http://www-hera-b.desy.de/subgroup/detector/rich/rich/lens_system Filename: plastic_trans.ps>
2012.
- 12 Franke, E. *et al.* In situ infrared and visible-light ellipsometric investigations of boron nitride thin
films at elevated temperatures. *J. Appl. Phys.* **1998**, *84*, 526-532.
- 13 Jackson, J. D. *Classical Electrodynamics*. John Wiley & Sons, **1999**.